Effects of Pressure on Diffusion and Vacancy Formation in MgO from Nonempirical Free-Energy Integrations

Joel Ita and Ronald E. Cohen
Geophysical Laboratory and Center for High Pressure Research, Carnegie Institution of Washington,
5251 Broad Branch Road, NW, Washington, D.C. 20015-1305

(Received 23 May 1997)

The free energies of vacancy pair formation and migration in MgO were computed via molecular dynamics using free-energy integrations and a nonempirical ionic model with no adjustable parameters. The intrinsic diffusion constant for MgO was obtained at pressures from 0 to 140 GPa and temperatures from 1000 to 5000 K. Excellent agreement was found with the zero pressure diffusion data within experimental error. The homologous temperature model which relates diffusion to the melting curve describes well our high pressure results within our theoretical framework. [S0031-9007(97)04344-5]

PACS numbers: 61.72.Bb, 62.50.+p, 66.30.Dn, 91.60.Ed

Diffusion and vacancy formation are critical to kinetic processes in materials [1], yet little is known about diffusion at high pressures due to experimental difficulties. Rheology of oxide minerals at high pressures is also crucial in geophysics [2]. Deformation in the deep Earth is thought to be diffusive in nature [3] and only limited experimental data are available at elevated pressures. To date, the highest measurements made are below 15 GPa [4]. This limited pressure range makes it difficult to extract critical parameters such as the activation volume and pressure dependence on the prefactor. As a result many have depended on a homologous temperature scaling relation to estimate the impact of pressure and temperature on diffusion in a region where this relation is untested [5]. However, the parameter required in the homologous temperature formalism is constrained by limited data mostly below 2.3 GPa and temperatures below 1500 K [6]. Thus we have undertaken a theoretical study of high pressure diffusion in the simplest oxide, MgO. This is the first nonempirical computation of diffusion at high pressures.

In ionic systems such as MgO, the dominant intrinsic defect is the pair vacancy [7–9] with Mg and O sites vacant. Previous work on vacancies in MgO used pseudopotential computations [10] or lattice dynamics or the Mott-Littleton approach with a variety of semiempirical potentials [11,12]. The accuracy of quasiharmonic lattice dynamics calculations degrades above the Debye temperature and the Mott-Littleton procedure and pseudopotential computations were restricted to 0 K.

We used molecular dynamics (MD) with nonempirical potentials to determine the self-diffusion coefficient D where [7]

$$D = Z_f \frac{Z_m}{6} l^2 \nu \exp\left(- \frac{\Delta G_f / W - \Delta G_m}{k_b T} \right), \qquad (1)$$

Z_f is the number of equivalent ways of forming a vacancy type, Z_m is the number of equivalent diffusion paths, l is the jump distance, ν is the attempt frequency, ΔG_f and ΔG_m are the energies of formation and migration, respectively, and W is the solubility factor for polyatomic materials. If the sites are uncorrelated (Schottky defect), then, for rocksalt structured (B1) crystals such as MgO, $W = 2$, $Z_f = 1$, $Z_m = 12$. Highly correlated defects (bound pair) require $W = 1$ and $Z_f = 6$. Symmetry and energy considerations determine the value of Z_m. In either case, $l^2 = a^2/2$, where a is the cubic cell parameter.

We used the variational induced breathing (VIB) model which reliably gives the thermal properties and equation of state of MgO [13] to compute the energetics and interatomic forces. The related potential induced breathing model was also used previously to study pressure effects on excitons in alkali halides giving good agreement with experiment and demonstrating that such models can give good defect properties for ionic materials [14]. The VIB model is a Gordon-Kim-type model [15] in which the total charge density is modeled by overlapping ionic charge densities which are computed using the local density approximation (LDA) [16]. The total energy is a sum of three terms: (a) the long-range electrostatic energy computed using the Ewald method, (b) the self-energy of each atom, and (c) the short-range interaction energy, the sum of the kinetic, short-range electrostatic and exchange-correlation energies from the LDA. There are three approximations beyond the LDA [17]: (i) The charge density is modeled rather than computed self-consistently. Comparisons with accurate linearized augmented plane wave computations show this is a good approximation for MgO [18]. (ii) The pair approximation is used for the short-range interactions (c) which is a good approximation as long as closed shell ions are used [19]. (iii) The Thomas-Fermi kinetic energy is used for the short-range overlap kinetic energy. The self-energy (b) includes the correct LDA Kohn-Sham kinetic energy. O^{2-} is not stable in the free state and is stabilized by introducing a sphere of 2+ charge (Watson sphere) around it in the LDA atomic calculations. Interactions are obtained for overlapping ion pairs at different distances with different Watson sphere radii on the O's. For efficiency, the interactions were fit with a 21 parameter analytical expression as functions of r, the interatomic distance, and $U_i = z_i/R_i$, where U_i, z_i, and R_i are the Watson sphere potential, charge (2+), and radius for atom i, respectively. During the simulations, the total energy was variationally optimized with respect to all of the Watson sphere radii at each time step.

The attempt frequency ν was determined by Fourier transforming the trajectories of the diffusing ion projected onto the shortest path to the vacancy. We considered two models: (1) the lowest frequency peak in the spectrum, assuming that the diffusive motion is mostly from the lowest energy mode and (2) the average frequency computed from the Fourier transform. In the first case we found that $\nu = 5.2$ THz and is independent of P and T over the range studied. The second case gave an attempt frequency that is within a factor of 2 of the low frequency value. Given the uncertainties in the calculations and experimental determinations, the difference in the final results between these two approaches is small and we adopted case (1) below.

Free energies were computed with the finite time variational or "adiabatic switching" thermodynamic integration method [20]. The free-energy difference between the initial and final states is

$$\Delta F = \int_0^1 \frac{\partial F(\lambda)}{\partial \lambda}\, d\lambda = \int_0^1 \left\langle \frac{\partial H(\lambda)}{\partial \lambda} \right\rangle_\lambda d\lambda\,, \tag{2}$$

where λ is a progress variable which ranges from 0 to 1 as the system "switches" from its initial to final state, H is the system Hamiltonian, and $\langle\,\rangle_\lambda$ represents an ensemble average. In order to obtain ΔG_f, we first calculated the free-energy difference between an ideal crystal at volume, V_I, giving the desired average P at T and an Einstein crystal at the same V and T. This was repeated for a defective crystal with a bound vacancy pair in each periodic cell at V_D corresponding to P. Then for an N atom periodic cell

$$\Delta G_f = F_D^{N-L}(V_D) - \frac{N-L}{N} F_I^N(V_I) + P\left[V_D - \frac{N-L}{N} V_I\right], \tag{3}$$

where $F_D^{N-L}(V_D)$ is the Helmholtz free energy of a defective crystal with L vacant sites and $F_I^N(V_I)$ is the Helmholtz free energy of the ideal crystal. The Hamiltonian took the form

$$H(\lambda) = H_{\rm VIB} \times (1-\lambda) + H_{\rm ein}\lambda\,, \tag{4}$$

where $H_{\rm ein}$ is the Hamiltonian for an Einstein crystal [21], which can be written as

$$H_{\rm ein} = K + U_0 + \sum_{i=1}^{N} \frac{1}{2} m_i \omega_{{\rm ein},i} (\overrightarrow{x_i} - \overrightarrow{x_{i0}})^2, \tag{5}$$

where K is the kinetic energy, U_0 is the static contribution to the potential, m_i, $\overrightarrow{x_i}$, $\overrightarrow{x_{i0}}$, and $\omega_{{\rm ein},i}$ are the mass, position, static lattice position, and Einstein frequency of the ith particle, respectively. The form of λ as a function of the scaled time, τ, is

$$\lambda(\tau) = \tau^5(70\tau^4 - 315\tau^3 + 540\tau^2 - 420\tau + 126)\,, \tag{6}$$

where $\tau = t/t_s$, t is the elapsed time, and t_s is the total switching time [21].

Migration free energies were calculated using the adiabatic switching procedure at constant P and T. We computed the energy it takes to push the atom out of one lattice site and into another vacant lattice site [22]. The force on the migrating atom due to $H_{\rm VIB}$ in the migration direction was set to zero and the negative of this force was evenly distributed among the rest of the atoms so that the force on the center of mass was zero. The position of the migrating atom was then incremented in the migration direction. Forces on the atom in the plane perpendicular to the migration direction were not artificially constrained so that the path the migrating atom took did not lie on a direct line between the initial position of the atom and the vacancy site. ΔG_m was determined by summing the difference in $H_{\rm VIB}$ before and after incrementing the position of the migrating atom with the other atomic positions held fixed. We found that the barriers to migration for ions that have a vacancy pair as a next-nearest neighbor are lower than those who have a vacancy pair as a nearest neighbor. Thus the value of Zm is 8 in MgO for correlated defects.

MD was performed using a time step of 1 fs with a fifth order Gear predictor-corrector scheme [23] in an isobaric-isothermal ensemble generated using the extended system method [24] for 10 ps equilibration times followed by a 10 (15) ps switching time for the formation (migration) energy. Convergence with respect to our nominal 216 atom system size was verified for systems with up to 1000 atoms to be within 1%. Doubling the integration time resulted in free-energy variations of 1% while halving it increased the calculated free-energy change by 10%. The computationally efficient first principles method used here lends itself to demanding convergence tests, especially with respect to system size, that would prove too time consuming with self-consistent methods [10].

Values of ΔG_f for bound pairs and ΔG_m are given in Table I. At 0 GPa, these energies are within 5% of those derived from previous theoretical and experimental results [8,9,11]. To determine the dominant vacancy mechanism, we calculated the binding energy ΔG_b of a bound pair from the difference in ΔG_f between bound vacancy pairs and those with the largest possible distance between vacant Mg and O sites in a 1000 atom supercell corrected for image forces [26] and found $\Delta G_b = 2.5 \times 10^{-19}$ J at 0 GPa and 2000 K and 7.0×10^{-19} J at 140 GPa and 3000 K. No significant changes in migration energy relative to the bound pair simulation were found. Assuming that the variation in binding energy is linear in pressure

TABLE I. Free energies of formation and migration and cell parameter.

P (GPa)	T (K)	ΔG_f (10^{-19} J)	a (Å)	ΔG_m (10^{-19} J) Mg	O
0	1000	8.19 ± 0.39	4.2495	3.36 ± 0.10	3.75 ± 0.11
0	2000	7.88 ± 0.23	4.3073	2.72 ± 0.12	3.16 ± 0.12
20	2000	12.04 ± 0.40	4.1312	3.75 ± 0.10	4.09 ± 0.10
20	3000	11.57 ± 0.56	4.1687	3.60 ± 0.10	4.06 ± 0.12
80	2000	21.20 ± 0.60	3.8610	5.16 ± 0.10	5.84 ± 0.17
80	3000	21.01 ± 0.90	3.8803	4.99 ± 0.11	5.86 ± 0.07
80	4000	20.75 ± 0.71	3.9031	4.55 ± 0.10	5.61 ± 0.16
140	2000	26.96 ± 0.82	3.7071	6.39 ± 0.10	6.91 ± 0.10
140	3000	25.29 ± 1.11	3.7210	5.99 ± 0.15	6.21 ± 0.21
140	5000	23.44 ± 1.76	3.7509	4.80 ± 0.30	5.69 ± 0.41

and independent of temperature and taking into account the configurational entropy, we calculated the vacancy concentration and Gibbs free-energy change for crystals containing bound and disassociated pairs relative to the perfect crystal [7]. This analysis shows that Schottky defects dominate at 1000 K or above due to entropy contributions (lower temperatures will favor the bound state). Ionic conductivity measurements indicate that Mg diffusion (D_{Mg}) is controlled by impurities [25], whereas O diffusion (D_{O}) is intrinsic in nature and directly comparable to our analysis. We find that our predicted D_{O} agrees with experiment within mutual error (Fig. 1).

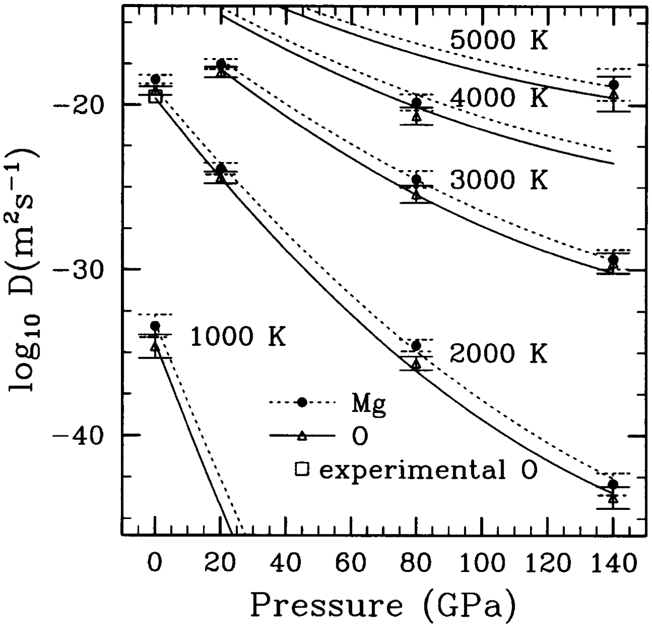

FIG. 1. Predicted pressure and temperature dependence of the self-diffusion coefficients in MgO. Curves represent the best fit to the coefficients using the activation energy-volume relation given by Eq. (7). Vertical symbol size of experimental datum taken from Ref. [9] represents uncertainty.

Fitting our diffusion constants with the relation

$$\ln D = \ln(a^2\nu) + S_0^* + PS_0^{*\prime} - (E_0^* + PV_0^* + P^2V_0^{*\prime})/k_bT \qquad (7)$$

gives the zero pressure activation entropy $S_0^* = 3\ (4)k_b$, its pressure derivative $S_0^{*\prime} = 0.03\ (0.02)k_b/\mathrm{GPa}$, activation energy $E_0^* = 900\ (940)\times10^{-21}$ J, activation volume $V_0^* = 16.0\ (16.7)$ Å^3, and its pressure derivative $V_0^{*\prime} = -0.031\ (0.038)$ Å^3/GPa for Mg (O). The activation volume varies as a function of pressure consistent with previous discussions [26–28]. The activation entropy is of the same order as previous estimates of the formation entropy at 0 GPa but varies much less drastically with pressure than a previous estimate [26].

Finally, we considered the homologous temperature relation

$$D = D_0 \exp(-gT_m/T) \qquad (8)$$

commonly used to model the dependence of diffusion on P and T [29]. Because of the similarity of behavior in diffusion of Mg and O, we used the effective diffusion coefficient, $D_{\mathrm{eff}} = 2D_{\mathrm{Mg}}D_{\mathrm{O}}/(D_{\mathrm{Mg}} + D_{\mathrm{O}})$ for D [30]. We tested this model using the theoretical melting curve of Cohen and Weitz [31] obtained with the same VIB potential as used here, and the extrapolated experimental melting curve of Zerr and Boehler [32] which has a lower dP/dT. Good global fits were found using the theoretical melting curve, but the experimental melting curve is not consistent with the present diffusion results. As discussed in Ref. [31] the experimental results may be influenced by Ar solubility in MgO melt at high pressures. Theoretical estimates of the melting curve are generally consistent with each other and with expected thermodynamic parameters.

We also tested the use of zero pressure diffusion results only in Eq. (8) and found that extrapolations to high pressure using the melting curve were reasonably reliable although some accuracy was lost compared to the results from direct high pressure simulations. This gives justification for use of melting curves in estimating high P and T diffusion in oxides.

In summary, we found (1) excellent agreement with experimental results, (2) that defects are formed from Schottky pairs as opposed to neutral divacancies, and (3) the homologous temperature relation holds within our theoretical framework. These results will help constrain rheological properties of the deep Earth and provide constraints for pressure effects on kinetics in oxides.

We thank W. P. Reinhardt and V. Heine for helpful discussions. This work was supported by NSF Grant No. EAR94-18934. Computations were performed on the Cray J916/12-1024 at the Geophysical Laboratory, CIW, purchased with support from NSF Grant No. EAR95-12627.

[1] M. J. Aziz, Appl. Phys. Lett. **70**, 2810 (1997).
[2] S. Karato and P. Li, Science **255**, 1238 (1992).
[3] P. Li, S. Karato, and Z. Wang, Phys. Earth Planet. Inter. **95**, 19 (1996).
[4] D. L. Farber, Q. Williams, and F. J. Ryerson, Nature (London) **371**, 693 (1994).
[5] P. E. van Keken, D. A. Yuen, and A. P. van den Berg, Science **264**, 1437 (1994).
[6] R. S. Borch and H. W. Green, Nature (London) **330**, 345 (1987).
[7] R. J. D. Tilley, *Defect Crystal Chemistry and Its Applications* (Blackie, Glasgow, London, 1987).
[8] K. Ando, in *Rheology of Solids and of the Earth,* edited by S. Karato and M. Toriumi (Oxford Univ. Press, Oxford, 1989).
[9] M. H. Yang and C. P. Flynn, Phys. Rev. Lett. **73**, 1809 (1994).
[10] A. De Vita, M. J. Gillan, J. S. Lin, M. C. Payne, I. Štich, and L. J. Clarke, Phys. Rev. B **46**, 12 964 (1992).
[11] L. Vočadlo, A. Wall, S. C. Parker, and G. D. Price, Phys. Earth Planet. Inter. **88**, 193 (1995).
[12] W. C. Mackrodt and R. F. Stewart, J. Phys. C **12**, 5015 (1979).
[13] I. Inbar and R. E. Cohen, Geophys. Res. Lett. **22**, 1533 (1995).
[14] H. Zhang, W. B. Daniels, and R. E. Cohen, Phys. Rev. B **50**, 70 (1994).
[15] R. G. Gordon and Y. S. Kim, J. Chem. Phys. **56**, 3122 (1972).
[16] R. E. Cohen, L. L. Boyer, and M. J. Mehl, Phys. Rev. B **35**, 5749 (1987).
[17] L. Hedin and B. I. Lundqvist, J. Phys. C **4**, 2064 (1971).
[18] M. J. Mehl, R. E. Cohen, and H. Krakauer, J. Geophys. Res. **93**, 8009 (1988).
[19] L. L. Boyer, M. J. Mehl, J. L. Feldman, J. R. Hardy, J. W. Flocken, and C. Y. Fong, Phys. Rev. Lett. **54**, 1940 (1985).
[20] J. E. Hunter, W. P. Reinhardt, and T. F. Davis, J. Chem. Phys. **99**, 6856 (1993).
[21] M. de Koning and A. Antonelli, Phys. Rev. E **53**, 465 (1996).
[22] V. Milman, M. C. Payne, V. Heine, R. J. Needs, J. S. Lin, and M. H. Lee, Phys. Rev. Lett. **70**, 2928 (1993).
[23] C. W. Gear, *Numerical and Initial Value Problems in Ordinary Differential Equations* (Prentice-Hall, Englewood Cliffs, NJ, 1971).
[24] G. J. Martyna, D. J. Tobias, and M. L. Klien, J. Phys. Chem. **101**, 4177 (1994).
[25] D. R. Sempolinski and W. D. Kingery, J. Am. Ceram. Soc. **63**, 664 (1980).
[26] D. R. Mills, S. C. Parker, and A. Wall, Philos. Mag. A **64**, 1133 (1991).
[27] S. Karato, Phys. Earth Planet. Inter. **24**, 1 (1981).
[28] J. P. Poirier and R. C. Liebermann, Phys. Earth Planet. Inter. **35**, 283 (1984).
[29] C. G. Sammis, J. C. Smith, and G. Schubert, J. Geophys. Res. **86**, 10 707 (1981).
[30] J. P. Poirier, *Creep of Crystals* (Cambridge University Press, Cambridge, England, 1985).
[31] R. E. Cohen and J. S. Weitz, in High Pressure-Temperature Research: Properties of Earth and Planetary Materials, edited by M. H. Manghnani and T. Yagi (American Geophysical Union, Washington, DC, to be published).
[32] A. Zerr and R. Boehler, Nature (London) **371**, 506 (1994).